A Conserved Role of the Unconventional Myosin 1d in Laterality Determination

Melanie Tingler, Sabrina Kurz, Markus Maerker, Tim Ott, Franziska Fuhl, Axel Schweickert, Janine Leblanc-Straceski, Stéphane Noselli, Martin Blum

Report

Current Biology

A Conserved Role of the Unconventional Myosin 1d in Laterality Determination

Graphical Abstract

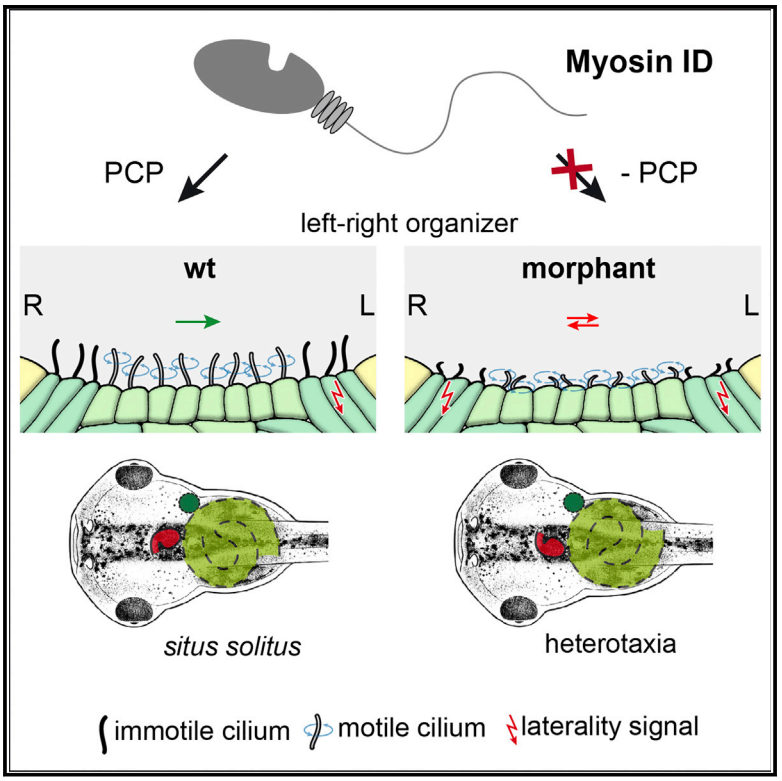

Highlights

- The unconventional myosin 1D is required for vertebrate left-right asymmetry
- Loss of *myo1d* causes aberrant leftward flow and laterality defects in *Xenopus*
- The function of myosin1D is mediated through the planar cell polarity pathway
- Myosin 1D links laterality in arthropods and chordates

Authors

Melanie Tingler, Sabrina Kurz, Markus Maerker, ..., Janine M. LeBlanc-Straceski, Stéphane Noselli, Martin Blum

Correspondence

martin.blum@uni-hohenheim.de

In Brief

Tingler et al. show that myosin 1D is required for laterality in the frog *Xenopus*, namely for left-asymmetric gene expression and leftward flow. Myosin 1D acts through the planar cell polarity pathway, a key feature of asymmetric gonad and gut morphogenesis in *Drosophila*, suggesting a common evolutionary origin of arthropod and chordate laterality.

Tingler et al., 2018, Current Biology *28*, 810–816
March 5, 2018
https://doi.org/10.1016/j.cub.2018.01.075

CellPress

CellPress

Current Biology
Report

A Conserved Role of the Unconventional Myosin 1d in Laterality Determination

Melanie Tingler,[1,4] Sabrina Kurz,[1,4] Markus Maerker,[1,4] Tim Ott,[1,4] Franziska Fuhl,[1,4] Axel Schweickert,[1] Janine M. LeBlanc-Straceski,[2] Stéphane Noselli,[3] and Martin Blum[1,5,*]
[1]University of Hohenheim, Institute of Zoology, Garbenstrasse 30, 70593 Stuttgart, Germany
[2]Department of Biology, Merrimack College, 315 Turnpike Street, North Andover, MA 01845, USA
[3]Université Côte d'Azur, CNRS, INSERM, Institut de Biologie Valrose, Parc Valrose, 06108 Nice, France
[4]These authors contributed equally
[5]Lead Contact
*Correspondence: martin.blum@uni-hohenheim.de
https://doi.org/10.1016/j.cub.2018.01.075

SUMMARY

Anatomical and functional asymmetries are widespread in the animal kingdom [1, 2]. In vertebrates, many visceral organs are asymmetrically placed [3]. In snails, shells and inner organs coil asymmetrically, and in *Drosophila*, genitalia and hindgut undergo a chiral rotation during development. The evolutionary origin of these asymmetries remains an open question [1]. Nodal signaling is widely used [4], and many, but not all, vertebrates use cilia for symmetry breaking [5]. In *Drosophila*, which lacks both cilia and Nodal, the unconventional *myosin ID* (*myo1d*) gene controls dextral rotation of chiral organs [6, 7]. Here, we studied the role of *myo1d* in left-right (LR) axis formation in *Xenopus*. Morpholino oligomer-mediated *myo1d* downregulation affected organ placement in >50% of morphant tadpoles. Induction of the left-asymmetric Nodal cascade was aberrant in >70% of cases. Expression of the flow-target gene *dand5* was compromised, as was flow itself, due to shorter, fewer, and non-polarized cilia at the LR organizer. Additional phenotypes pinpointed Wnt/planar cell polarity signaling and suggested that *myo1d*, like in *Drosophila* [8], acted in the context of the planar cell polarity pathway. Indeed, convergent extension of gastrula explant cultures was inhibited in *myo1d* morphants, and the *ATF2* reporter gene for non-canonical Wnt signaling was downregulated. Finally, genetic interference experiments demonstrated a functional interaction between the core planar cell polarity signaling gene *vangl2* and *myo1d* in LR axis formation. Thus, our data identified *myo1d* as a common denominator of arthropod and chordate asymmetry, in agreement with a monophyletic origin of animal asymmetry.

RESULTS AND DISCUSSION

The Unconventional *myosinID* Gene Is Required for LR Axis Formation in *Xenopus laevis*

We have previously shown that maternal and zygotic Myo1d is present in the *Xenopus* egg cell and throughout the first 3 days of embryogenesis [9], i.e., before, during, and after left-right (LR) symmetry breaking [5]. Zygotic mRNA expression was predominantly found in presomitic mesoderm and somites [9], tissues related to the *Xenopus* LR organizer (LRO) [5]. To assess a possible function of *myo1d* in *Xenopus* LR axis formation, an antisense morpholino oligomer (MO) was designed that targeted sequences overlapping the translational start site (AUG-MO). AUG-MO was injected at the 4-cell stage and targeted toward the LRO. Specimens were cultivated until they reached stages 24, 32, or 45 to investigate *nodal1* or *pitx2* expression and organ situs, respectively. Organ placement, as assessed by heart and gut looping as well as positioning of the gall bladder (Figure 1A), was significantly disturbed in specimens injected with AUG-MO (Figures 1B–1D). Likewise, left-asymmetric expression of *nodal1* and *pitx2* were disturbed in >70% of AUG-MO-injected morphants, with bilateral expression in the left and right lateral plate mesoderm (LPM) representing the most commonly observed defective pattern (Figures 1E and 1F; Figures S1A–S1H). Remarkably, AUG-MO caused phenotypes at very low doses (0.2 pmol or 3.3 ng per embryo). Furthermore, a scrambled mismatch MO (MM-MO) did not affect the laterality of injected embryos (Figures 1E and 1F). In addition, Myo1d protein was downregulated in morphant embryos, as shown by western blot analysis (Figure S1I). A full-length *myo1d* expression construct [10] that was not targeted by AUG-MO partially rescued left-asymmetric *nodal1* expression in the LPM (Figure 1E). Together, these experiments argue for MO specificity. Bilateral *nodal1*/*pitx2* expression, observed in the majority of LR-altered *myo1d* morphants (75%; *cf.* Figures 1E and 1F), also occurs when the midline barrier function is disturbed [11], i.e., when Nodal1 protein crosses from the left to the right side. However, the midline in *myo1d* morphants was normal, as shown by the wild-type expression pattern of the midline barrier gene *lefty1* (Figures S1J and S1K).

To confirm the MO-derived LR phenotypes, we created CRISPR/Cas9 F0 mutants in *Xenopus laevis*. Two guide RNAs were designed, targeting subdomains of the ATP-binding site

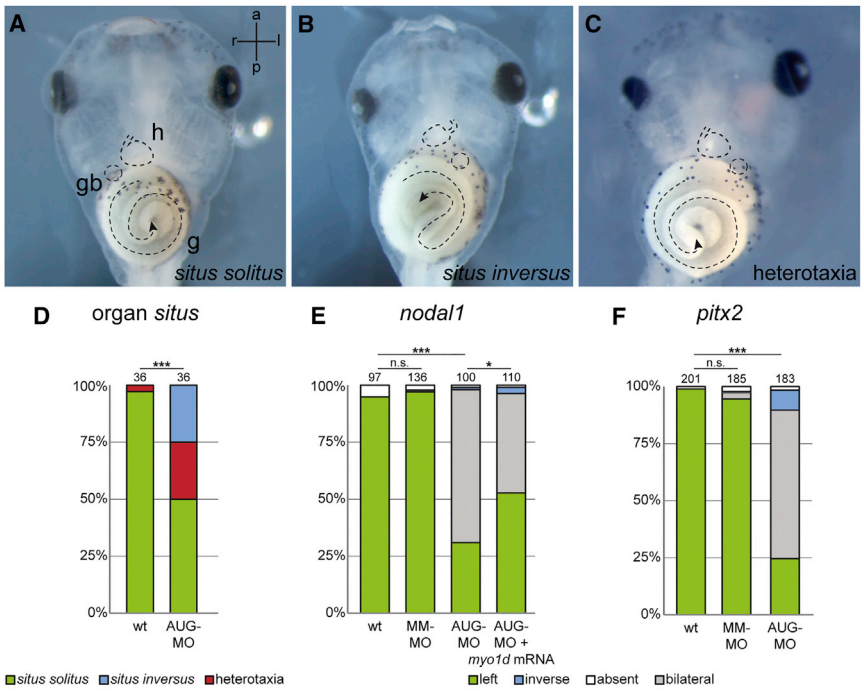

Figure 1. *myo1d* Is Required for LR Axis Formation in *Xenopus laevis*

(A–D) Organ situs in wild-type (A) and *myo1d* morphant tadpoles displaying situs inversus (B) and heterotaxia (C) at stage 45. g, gut; gb, gall bladder, h, heart.

(D) Quantification of organ situs analysis.

(E and F) Quantification of *nodal1* (E) and *pitx2* (F) expression patterns in wildtype embryos and specimens injected with MM-MO, AUG-MO or co-injected with AUG-MO and rescue mRNA. Numbers represent analyzed specimens, which were derived from 3 (D and E) and 5 (F) independent experiments.

See also Figure S1.

(Figure 2A), which were separately co-injected together with Cas9 protein into 1-cell-stage embryos [12]. Both resulted in identical ranges of phenotypes (Figures 2B and 2C): at least half the embryos were severely malformed, with gastrulation and blastopore closure defects, preventing the analysis of marker gene expression. Importantly, these phenotypes were encountered upon the injection of high doses of AUG-MO as well (data not shown). The remaining injected F0 specimens were evaluated for *pitx2* expression. About 60% lacked asymmetry and showed absent or bilateral *pitx2* expression (Figure 2D); remarkably, these embryos were also stunted, i.e., revealed a convergence extension phenotype (Figure 2C). The remaining specimens appeared normal and displayed left-asymmetric *pitx2* expression (Figures 2C and 2D). F0 *myo1d* mutants thus closely resembled *myo1d* morphants, as in both cases asymmetric marker gene expression was lost. Differences were recorded, however, namely that in morphants, Nodal cascade gene expression was bilateral in the vast majority of cases, while it was absent or bilateral in mutants. Although we lack a conclusive explanation at this time, beyond realizing that gene knockdowns differ from mosaic F0 mutants, genome editing provided additional proof of MO specificity, as in both cases the same quality of LR defect was observed, i.e., loss of asymmetry. In summary, these experiments demonstrated a role for *myo1d* in LR axis formation in *Xenopus*.

myo1d Is Required for LRO Morphogenesis and Leftward Flow

Induction of the left-asymmetric Nodal cascade in the LPM of the 2-day embryo is preceded by several well-defined morphogenetic and molecular steps, beginning with the specification of the LRO precursor, the so-called superficial mesoderm (SM), which forms caudal to the Spemann organizer at mid-gastrula stages [5, 13] (Figure S2A). The SM was not affected in *myo1d* morphants, as demonstrated by the expression of marker genes *foxj1* and *wnt11b* [14] (Figures S2B–S2E). The LRO in the frog is represented by the transient ciliated epithelium of the gastrocoel roof plate (GRP), which forms at the dorsal-posterior end of the primitive gut when SM cells involute during gastrulation [13, 15] (Figure S2A). We investigated whether the GRP had correctly formed in *myo1d* morphants using a Tektin isoform marker gene; *tekt2* expression was unaffected (Figures S2F and S2G), indicating that a GRP had formed. LRO function of the GRP arises when cilia develop and polarize in the central region of the GRP. As they become motile, they produce a leftward flow of extracellular fluids [16], which, presumably, is sensed by peripheral GRP cells harboring non-polarized and immotile cilia [1, 5].

To assess GRP morphogenesis, dorsal explants were prepared and analyzed for cilia by immunofluorescence (IF) using an antibody against acetylated alpha-tubulin. Figures 3A–3E show that, although cilia were present in morphant GRPs, ciliation was markedly altered. Cilia were significantly shorter, showed reduced polarization to the posterior pole of cells (a prerequisite of leftward flow), and were reduced in number (Figures 3F–3H). To determine if the flow itself was compromised, the transport of fluorescent microbeads was assessed using high-speed videography [16]. Time-lapse movies of GRPs show that flow was indeed disordered in *myo1d* morphants compared to wild-type specimens (Movie S1). Evaluation of flow parameters confirmed this disruption, with significantly reduced flow velocity and directionality in *myo1d* morphant specimens (Figures 3I and 3J). Importantly, some individual beads showed inverted movement, i.e., from left to right (Movie S1), in agreement with the observed predominant bilateral induction of asymmetric LPM marker genes (*cf.* Figures 1E and 1F). Leftward flow induces asymmetric LPM gene expression by downregulating the Nodal repressor *dand5* in lateral GRP cells (i.e., the purported flow sensor cells), where this gene is co-expressed with *nodal1* [17]. Expression of both genes was analyzed in dorsal explants isolated at post-flow stages (stage 19). Figures 3K–3O show that *nodal1* was unaffected in morphants, while *dand5* asymmetries were lost due to bilateral downregulation of mRNA expression. Expression of the

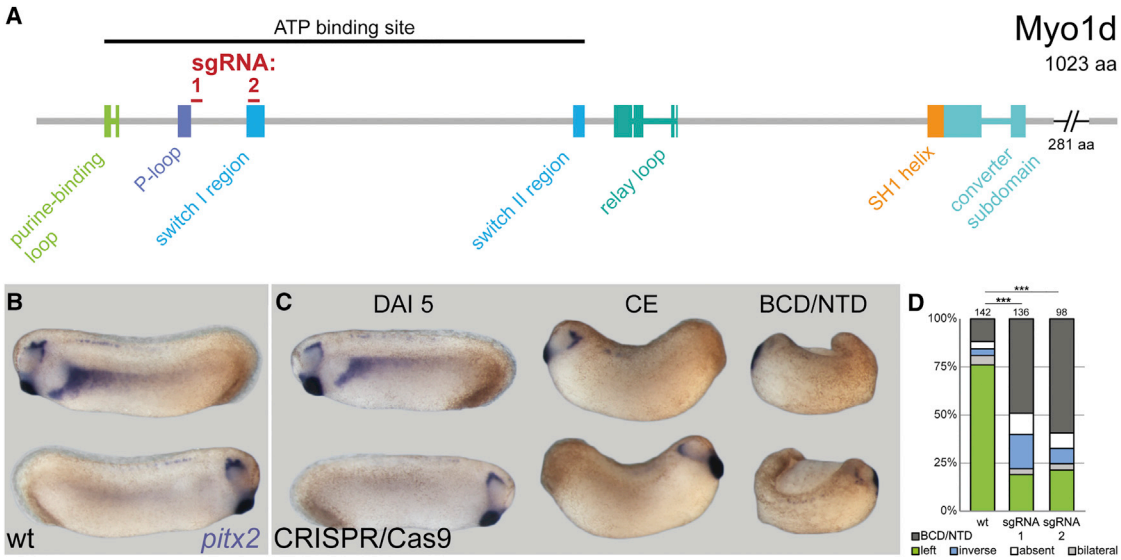

Figure 2. Laterality Defects in Genome-Edited F0 *myo1d* Mutant Tadpoles

(A) Schematic depicting Myo1d protein structure (sgRNA sites indicated).

(B and C) Appearance and *pitx2* gene expression in WT (B) and F0 *myo1d* mutant (C) tadpoles.

(D) Compilation of *pitx2* expression patterns. BCD, blastopore closure defect; NTD, neural tube closure defect. Note that mutant embryos with WT appearance showed WT *pitx2* expression in the left LPM, while stunted specimens with a convergent extension (CE) phenotype lacked expression or displayed mRNA expression on both sides.

transforming growth factor β (TGF-β) gene *gdf3*, the functional frog homolog of the Nodal agonist *Gdf1* in mouse, was unaltered in morphants (Figures S2H and S2I). In summary, these results demonstrated that *myo1d* was required for GRP morphogenesis and leftward flow and that downregulation of this conserved unconventional myosin resulted in a loss of molecular asymmetries and, consequently, a high frequency of heterotaxia (*situs ambiguus*) and *situs inversus* in morphant tadpoles (Figure 1).

PCP Defects in *myo1d* Morphant Frog Embryos

In *Drosophila*, *myo1d* interacts with both the global (Dachsous/Fat) and core (Frizzled/Wnt) PCP pathways to control chiral morphogenesis of the adult hindgut [8]. In the course of analyzing *myo1d* morphant *Xenopus* embryos, we noted a number of LR-unrelated developmental defects that have been linked to altered PCP signaling. First, the apical surface of GRP cells appeared enlarged in morphants as compared to wild-type (WT), suggesting a defect in apical constriction of involuting SM cells (*cf.* Figures 2A–2E). Apical constriction during gastrulation and neural tube closure is under the control of PCP [18]. Quantification of 25 cells each from 15 WT and 15 morphant embryos revealed that, on average, the cell surface in *myo1d* morphants was increased by 25% (Figure 4A). Second, neural tube closure was delayed in morphant embryos, i.e., the neural tube was still open at stage 18 when it had just closed in wild-type specimens (Figure 4B; Figures S3A and S3B; Movie S2). Delayed neural tube closure has been reported in the frog upon knockdown of *dishevveled2* (*dsh2*) and characterized as a convergent-extension (CE) defect that fails to narrow the midline [19]. In mouse embryos lacking one or both copies of the core PCP gene *vangl2*, the same phenotype was described [20]. Third, the ciliation of multi-ciliated cells (MCCs) in the larval skin of *myo1d* morphants was delayed. Ciliation of MCCs was much reduced on the morphant side of unilaterally injected stage 24 embryos, compared to the uninjected contralateral side (Figure S3C). No differences were recorded at stage 32, i.e., this phenotype represented a transient delay in MCC differentiation and apical intercalation (data not shown). MCC function was directly assessed by tracking fluorescent microbeads added to tadpoles. Figure 4C and Movies S3 and S4 demonstrate that defects observed at stage 24 were no longer present at stage 32 (data not shown). Such a transient delay in cilia extension of MCCs has previously been described upon *Foxn4* loss of function in *Xenopus* [21], and radial cell intercalation of MCC has been linked to PCP proteins Vangl2, Prickle3, and Disheveled [22]. Finally, the stunted appearance of F0 mutants with disturbed *pitx2* expression was reminiscent of a CE phenotype as well (*cf.* Figure 2C). Together, this evidence hinted at a more general role of *myo1d* in PCP signaling and CE.

To investigate *myo1d* function in the context of a well-established CE-Wnt/PCP assay, we employed Keller open-face explants [23]. Dorsal marginal zone tissue was isolated at stage 10–10.5 from WT and *myo1d* morphant embryos, and it was scored for CE when un-manipulated siblings reached stage 22 (Figure 4C). CE was classified into three categories, with class 0 representing explants without elongation, class 1 containing elongated specimens, and class 2 explants being those that were elongated and displayed a constriction (Figure 4C). While more than 90% of WT explants elongated, with the relative majority of specimens falling into class 2 (23/54, 43%), CE was severely compromised in *myo1d* morphants, with significantly reduced class 2 extensions (6/44), the relative majority of specimens elongating without constriction, and about 25% not

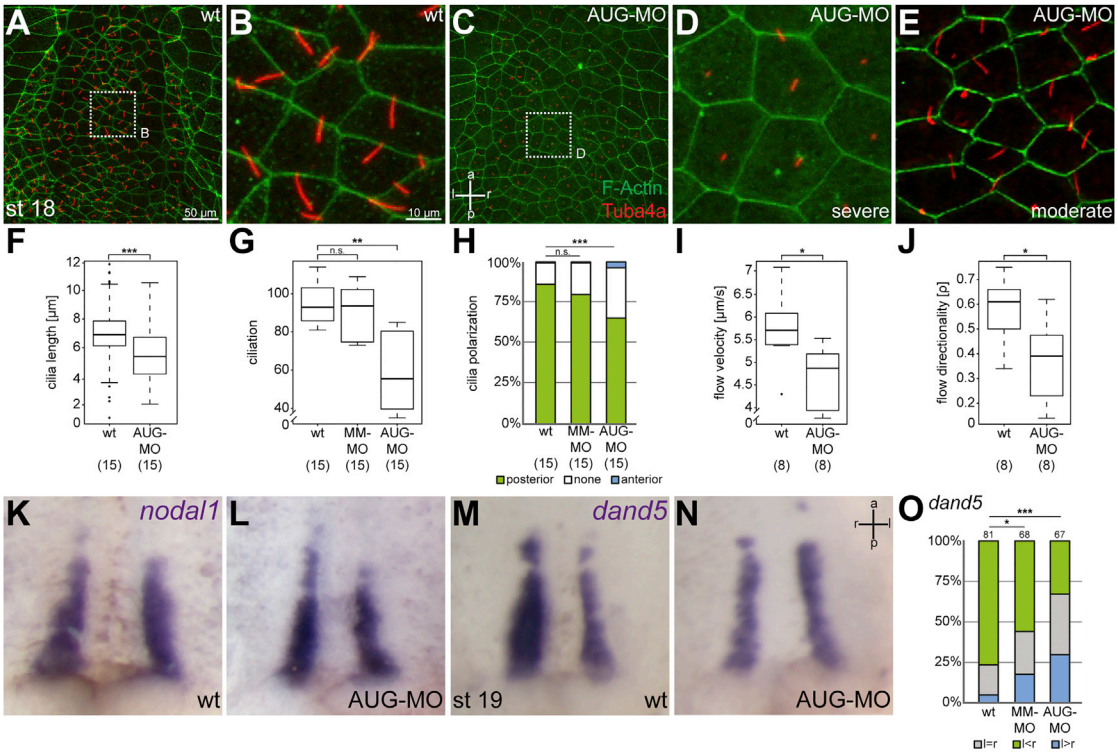

Figure 3. *myo1d* Is Required for GRP Morphogenesis and Leftward Flow

(A–E) GRP ciliation. Dorsal explants were prepared and analyzed for the presence and polarization of cilia by immunofluorescence using an antibody against acetylated alpha-tubulin. Counterstaining of actin using Phalloidin highlighted cell boundaries.

(A) Wild-type (blow-up shown in B).

(C) *myo1d* morphant.

(D and E) Blowups of severe phenotype shown in (D) and of moderate phenotype shown in (E).

(F–J) Quantification of cilia lengths (F), ciliation rate (G), cilia polarization (H), flow velocity (I), and flow directionality (J).

(K and L) Wild-type expression of *nodal1* in control (K) and *myo1d* morphant (L) stage 19 embryo.

(M–O) Asymmetrical *dand5* expression in lateral GRP cells of wild-type control embryo (M) was lost in *myo1d* morphant specimen (N).

(O) Quantification of *dand5* expression patterns.

(K)–(N) are shown at the same magnification.

Numbers represent analyzed specimens, which were derived from 3 (A–H), 2 (I and J), and 5 (K–O) independent experiments. For the assessment of cilia polarization, 15 cilia were analyzed per explant, for cilia lengths 30 cilia per GRP, and the ciliation rate was determined upon evaluating the entire GRP. See also Figure S2 and Movie S1.

elongating at all (class 1, 24/44, 61%; Figure 4C). Finally, an *ATF2*-based luciferase reporter was analyzed to monitor non-canonical Wnt signaling in *Xenopus* [24]. The reporter gene, alone or in combination with different concentrations of *myo1d* AUG-MO, was injected into the neural lineage at the 4-cell stage, neural plate explants were prepared at stage 14/15, and luciferase activity was recorded (Figure S3D). Compared to WT specimens, the reporter gene activity was dose-dependently downregulated in morphants (Figure S3D). In summary, these analyses of LR-unrelated phenotypes demonstrated that *myo1d* acted on non-canonical Wnt/PCP signaling and CE in the broader sense.

Functional Interaction between the Core PCP Signaling Gene *vangl2* and *myo1d* in LR Axis Formation in *Xenopus*

Finally, we asked whether PCP signaling and *myo1d* interacted during LR axis specification. Knockdown of the core PCP gene *vangl2* in *Xenopus* has been shown to disrupt cilia polarization and LPM *nodal1* expression [25]. For gene knockdown of *vangl2*, a combination of two previously characterized antisense MOs was injected [26]. To analyze the potential genetic interaction of *vangl2* and *myo1d*, MO doses were reduced such that individual knockdowns resulted in greatly attenuated phenotypes. When MOs were co-injected, LR phenotypes were observed, as documented for the expression of LPM *pitx2* (Figure 4D). These experiments unequivocally showed that *myo1d* was required for PCP-dependent determination of the LR axis in *Xenopus* in much the same way as in the fruit fly *Drosophila* [8]. A possible role of *myo1d* has been previously addressed by overexpression of a full-length expression construct [10]. Injections of high amounts of synthetic *myo1d* mRNAs ($\geq$5 ng) resulted in 15% of specimens with heterotaxia, but the mechanism of action was not addressed in this study [10]. We were not able to reproduce this result; it is a hallmark of non-canonical Wnt signaling and PCP, however, that both gain- and loss-of-function manipulations result in qualitatively similar phenotypes [27].

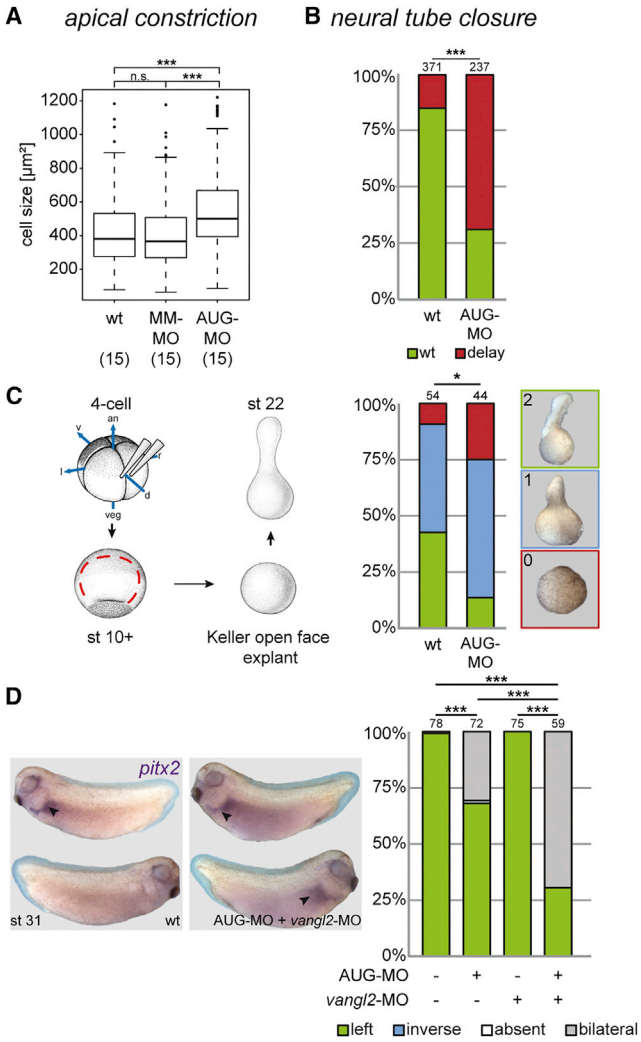

Figure 4. Functional Interaction between *myo1d* and PCP

(A and B) Morphant specimens displayed enhanced apical surfaces of GRP cells at stage 18 (A) and delayed neural tube closure at stage 18 (B).

(C) Convergent extension defects in Keller open-face explants of *myo1d* morphants at stage 22.

(D) Co-injection of *myo1d* AUG-MO with two antisense MOs directed against *vangl2* (at sub-phenotypic doses each) disrupted LR axis formation, as determined by expression of *pitx2* in the LPM. Numbers represent analyzed specimens, which were derived from 3 independent experiments for apical constriction defects of GRP cells, 7 experiments for neural tube closure delay, and 4 experiments for *myo1d* and *vangl2* interaction during LR axis formation. To determine the cell surface area, 25 cells from a central part of the GRP were analyzed in each case.

See also Figure S3 and Movies S2, S3, and S4.

The evolutionary origin of animal asymmetries has been controversially discussed in recent years [1, 28–30]. While morphological and functional asymmetries have been described in most phyla [1], there is no single common mechanism that accounts for asymmetric development. The Nodal cascade genes *nodal*, *lefty*, and *pitx2* are present and required for asymmetric development in lophotrochozoans (such as snails) and deuterostomes (sea urchins, uro- and cephalochordates as well as vertebrates), but they have not been described in ecdysozoans [1]. Cilia-driven leftward fluid flow at the LR organizer is a hallmark of some, but not all, chordates [1], and *Drosophila* as the sole ecdysozoan species studied in depth lacks Nodal and cilia but uses Myo1d, PCP, and the Hox gene *Abd-B* [7, 8] to achieve laterality. This diversity has been taken as evidence of multiple independent evolutionary pathways to establish LR asymmetry [31, 32].

Our finding of a role of *myo1d* in *Xenopus* LR development represents the first demonstration of a common denominator of ecdysozoan and deuterostome/chordate asymmetries. Interestingly, actomyosin-dependent asymmetric heart morphogenesis has recently been shown to depend on a right-sided instructive pathway that involves BMP signaling and, as a target, the homeobox gene *prrx1* [33]. It has been proposed that this BMP-Prrx1-actomyosin pathway is suggestive of a conserved role in laterality determination during bilaterian evolution [33], a notion that is fully supported by our data. Future studies will address the question of whether or not *myo1d* is involved in this pathway. Additionally, we uncovered a conserved link between PCP and *myo1d* in establishing LR asymmetry in flies and frogs. Interestingly, these results can be further generalized, as LR defects were also encountered in morphant and mutant CRISPR/Cas9 zebrafish embryos (S.N. and Max Furthauer, personal communication). Defects in zebrafish included shorter and mispolarized cilia, LRO morphogenetic defects, and aberrant leftward flow, resulting in absent Nodal cascade gene induction and organ situs distortions, and, most significantly, a genetic interaction with *vangl2* as well (S.N. and Max Furthauer, personal communication).

In conclusion, our data are consistent with a monophyletic origin of animal organ asymmetries. It may be beneficial to investigate other mechanisms of invertebrate asymmetries in vertebrate model organisms in the future (for which the frog *Xenopus* is particularly well suited [34]), such as the role of Hox genes, which may be involved in placing the LRO at the correct anterior-posterior position during development.

STAR★METHODS

Detailed methods are provided in the online version of this paper and include the following:

- KEY RESOURCES TABLE
- CONTACT FOR REAGENT AND RESOURCE SHARING
- EXPERIMENTAL MODEL AND SUBJECT DETAIL
- METHOD DETAILS
  - Plasmid construction
  - Immunfluorescence staining
  - Flow-analysis
  - Luciferase Assay
  - CRISPR/Cas9 mediated genome editing
  - Monoclonal Antibody Preparation
  - Western blot analysis
- QUANTIFICATION AND STATISTICAL ANALYSIS
  - Statistical analysis

SUPPLEMENTAL INFORMATION

Supplemental Information includes three figures and four movies and can be found with this article online at https://doi.org/10.1016/j.cub.2018.01.075.

ACKNOWLEDGMENTS

We are grateful to Michael Levin for sharing a full-length *myo1d* expression construct and to Susanne Bogusch, whose expert help was instrumental to cloning the rescue vector. Work in the Blum lab has been supported by DFG grants BL-285/9 and BL-285/10. S.K. and T.O. have been recipients of fellowships from the Landesgraduiertenförderung Baden-Württemberg. S.K. was also funded by the Federal Ministry of Education and Research (01PL11003), project Humboldt reloaded. J.M.L.-S. gratefully acknowledges several students in her 1998–2015 Molecular Biology and Biotechnology and Directed Research courses, especially G. Angelini, K. Ganser, S. Saldi, N. McIver, and B. Sickler; the Merrimack College Faculty Development Grant Program; Murray Fellowship; Yassini Award; NSF-RUI 0077516; and B. Bement, A. Sokac, S. Sokol, and members of his laboratory. Work in the Noselli lab was supported by grants from ANR (DRO-ASY ANR-13-BSV2-006, DroZeMyo, and LABEX SIGNALIFE ANR-11-LABX-0028-01).

AUTHOR CONTRIBUTIONS

M.B., M.T., A.S., and S.N. designed experiments. M.T., S.K., M.M., F.F., and J.M.L.-S. conducted experiments, with T.O. performing the CRISPR/Cas9 genome editing. M.B. wrote the manuscript with help from M.T., A.S., S.N., and J.M.L.-S.

DECLARATION OF INTERESTS

The authors declare no competing interests.

Received: October 19, 2017
Revised: January 1, 2018
Accepted: January 24, 2018
Published: February 22, 2018

REFERENCES

1. Blum, M., Feistel, K., Thumberger, T., and Schweickert, A. (2014a). The evolution and conservation of left-right patterning mechanisms. Development *141*, 1603–1613.
2. Coutelis, J.B., González-Morales, N., Géminard, C., and Noselli, S. (2014). Diversity and convergence in the mechanisms establishing L/R asymmetry in metazoa. EMBO Rep. *15*, 926–937.
3. Grimes, D.T., and Burdine, R.D. (2017). Left-Right Patterning: Breaking Symmetry to Asymmetric Morphogenesis. Trends Genet. *33*, 616–628.
4. Shiratori, H., and Hamada, H. (2014). TGFβ signaling in establishing left-right asymmetry. Semin. Cell Dev. Biol. *32*, 80–84.
5. Blum, M., Schweickert, A., Vick, P., Wright, C.V.E., and Danilchik, M.V. (2014b). Symmetry breakage in the vertebrate embryo: when does it happen and how does it work? Dev. Biol. *393*, 109–123.
6. Hozumi, S., Maeda, R., Taniguchi, K., Kanai, M., Shirakabe, S., Sasamura, T., Spéder, P., Noselli, S., Aigaki, T., Murakami, R., and Matsuno, K. (2006). An unconventional myosin in Drosophila reverses the default handedness in visceral organs. Nature *440*, 798–802.
7. Spéder, P., Adám, G., and Noselli, S. (2006). Type ID unconventional myosin controls left-right asymmetry in Drosophila. Nature *440*, 803–807.
8. González-Morales, N., Géminard, C., Lebreton, G., Cerezo, D., Coutelis, J.-B., and Noselli, S. (2015). The Atypical Cadherin Dachsous Controls Left-Right Asymmetry in Drosophila. Dev. Cell *33*, 675–689.
9. LeBlanc-Straceski, J.M., Sokac, A., Bement, W., Sobrado, P., and Lemoine, L. (2009). Developmental expression of Xenopus myosin 1d and identification of a myo1d tail homology that overlaps TH1. Dev. Growth Differ. *51*, 443–451.
10. McDowell, G.S., Lemire, J.M., Paré, J.-F., Cammarata, G., Lowery, L.A., and Levin, M. (2016). Conserved roles for cytoskeletal components in determining laterality. Integr. Biol. *8*, 267–286.
11. Meno, C., Shimono, A., Saijoh, Y., Yashiro, K., Mochida, K., Ohishi, S., Noji, S., Kondoh, H., and Hamada, H. (1998). lefty-1 is required for left-right determination as a regulator of lefty-2 and nodal. Cell *94*, 287–297.
12. Nakayama, T., Blitz, I.L., Fish, M.B., Odeleye, A.O., Manohar, S., Cho, K.W.Y., and Grainger, R.M. (2014). Cas9-based genome editing in Xenopus tropicalis. Methods Enzymol. *546*, 355–375.
13. Shook, D.R., Majer, C., and Keller, R. (2004). Pattern and morphogenesis of presumptive superficial mesoderm in two closely related species, Xenopus laevis and Xenopus tropicalis. Dev. Biol. *270*, 163–185.
14. Walentek, P., Schneider, I., Schweickert, A., and Blum, M. (2013). Wnt11b is involved in cilia-mediated symmetry breakage during Xenopus left-right development. PLoS ONE *8*, e73646.
15. Blum, M., Andre, P., Muders, K., Schweickert, A., Fischer, A., Bitzer, E., Bogusch, S., Beyer, T., van Straaten, H.W.M., and Viebahn, C. (2007). Ciliation and gene expression distinguish between node and posterior notochord in the mammalian embryo. Differentiation *75*, 133–146.
16. Schweickert, A., Weber, T., Beyer, T., Vick, P., Bogusch, S., Feistel, K., and Blum, M. (2007). Cilia-driven leftward flow determines laterality in Xenopus. Curr. Biol. *17*, 60–66.
17. Schweickert, A., Vick, P., Getwan, M., Weber, T., Schneider, I., Eberhardt, M., Beyer, T., Pachur, A., and Blum, M. (2010). The nodal inhibitor Coco is a critical target of leftward flow in Xenopus. Curr. Biol. *20*, 738–743.
18. Ossipova, O., Chuykin, I., Chu, C.-W., and Sokol, S.Y. (2015b). Vangl2 cooperates with Rab11 and Myosin V to regulate apical constriction during vertebrate gastrulation. Development *142*, 99–107.
19. Wallingford, J.B., and Harland, R.M. (2002). Neural tube closure requires Dishevelled-dependent convergent extension of the midline. Development *129*, 5815–5825.
20. Ybot-Gonzalez, P., Savery, D., Gerrelli, D., Signore, M., Mitchell, C.E., Faux, C.H., Greene, N.D.E., and Copp, A.J. (2007). Convergent extension, planar-cell-polarity signalling and initiation of mouse neural tube closure. Development *134*, 789–799.
21. Campbell, E.P., Quigley, I.K., and Kintner, C. (2016). Foxn4 promotes gene expression required for the formation of multiple motile cilia. Development *143*, 4654–4664.
22. Ossipova, O., Chu, C.-W., Fillatre, J., Brott, B.K., Itoh, K., and Sokol, S.Y. (2015a). The involvement of PCP proteins in radial cell intercalations during Xenopus embryonic development. Dev. Biol. *408*, 316–327.
23. Sive, H.L., Grainger, R.M., and Harland, R.M. (2007). Xenopus laevis Keller Explants. CSH Protoc. *2007*, pdb.prot4749.
24. Ohkawara, B., and Niehrs, C. (2011). An ATF2-based luciferase reporter to monitor non-canonical Wnt signaling in Xenopus embryos. Dev. Dyn. *240*, 188–194.
25. Antic, D., Stubbs, J.L., Suyama, K., Kintner, C., Scott, M.P., and Axelrod, J.D. (2010). Planar cell polarity enables posterior localization of nodal cilia and left-right axis determination during mouse and Xenopus embryogenesis. PLoS ONE *5*, e8999.
26. Prager, A., Hagenlocher, C., Ott, T., Schambony, A., and Feistel, K. (2017). hmmr mediates anterior neural tube closure and morphogenesis in the frog Xenopus. Dev. Biol. *430*, 188–201.
27. Wang, Y., and Nathans, J. (2007). Tissue/planar cell polarity in vertebrates: new insights and new questions. Development *134*, 647–658.
28. Boorman, C.J., and Shimeld, S.M. (2002). The evolution of left-right asymmetry in chordates. BioEssays *24*, 1004–1011.
29. Thompson, H., Shaw, M.K., Dawe, H.R., and Shimeld, S.M. (2012). The formation and positioning of cilia in Ciona intestinalis embryos in relation to the generation and evolution of chordate left-right asymmetry. Dev. Biol. *364*, 214–223.
30. Nakamura, T., and Hamada, H. (2012). Left-right patterning: conserved and divergent mechanisms. Development *139*, 3257–3262.

31. Okumura, T., Utsuno, H., Kuroda, J., Gittenberger, E., Asami, T., and Matsuno, K. (2008). The development and evolution of left-right asymmetry in invertebrates: lessons from Drosophila and snails. Dev. Dyn. *237*, 3497–3515.

32. Vandenberg, L.N., and Levin, M. (2013). A unified model for left-right asymmetry? Comparison and synthesis of molecular models of embryonic laterality. Dev. Biol. *379*, 1–15.

33. Ocaña, O.H., Coskun, H., Minguillón, C., Murawala, P., Tanaka, E.M., Galcerán, J., Muñoz-Chápuli, R., and Nieto, M.A. (2017). A right-handed signalling pathway drives heart looping in vertebrates. Nature *549*, 86–90.

34. Duncan, A.R., and Khokha, M.K. (2016). Xenopus as a model organism for birth defects-Congenital heart disease and heterotaxy. Semin. Cell Dev. Biol. *51*, 73–79.

STAR★METHODS

KEY RESOURCES TABLE

REAGENT or RESOURCE	SOURCE	IDENTIFIER
Antibodies		
Mouse monoclonal anti acetylated α-tubulin	Sigma	T6793
Anti-mouse IgG (whole molecule) F(ab')2 fragment-Cy3	Sigma	C2181
Anti-mouse IgG (H+L), CF 405S	Sigma	SAB4600023
Alexa Fluor 488 Phalloidin	Invitrogen	A12379
Alexa Fluor 555 Phalloidin	Invitrogen	A34055
Chemicals, Peptides, and Recombinant Proteins		
Pfu DNA Polymerase	Promega	M7745
Cas9 with NLS	PNA BIO	CP01-50
FluoSpheres Carboxylate-Modified Microspheres, 0.5 μm, yellow-green fluorescent (505/515)	Invitrogen	F8813
Human chorionic gonadotropin (hCG)	Sigma	C0809-1VL
PureProteome NHS Flexibind Magnetic Beads	Milipore	LSKMAGA02
Laemmli sample buffer 2x	Sigma	S3401
Critical Commercial Assays		
MEGAshortscript T7 Transcription Kit	Thermo Fisher Scientific	AM1354
MEGAclear Transcription Clean-Up Kit	Thermo Fisher Scientific	AM1908
innuPREP DOUBLEpure Kit	Analytik Jena	845-KS-5050050
Ni-NTA affinity purification column	QIAGEN	N/A
EDTA-free Protease Inhibitor Cocktail	Roche	000000011873580001
Dual-Luciferase® Reporter Assay System	Promega	E1910
Experimental Models: Cell Lines		
BL21 Star One Shot cells	Invitrogen	C602003
Experimental Models: Organisms/Strains		
Xenopus laevis (female, male)	Nasco	https://www.enasco.com/xenopus/
Oligonucleotides		
sgRNA-RO: AAAAGCACCGACTCGGTGCCACTTTTTCAAGT TGATAACGGACTAGCCTTATTTTAACTTGCTATTTCTAGCT CTAAAAC	Merck	N/A
T7:sgRNA 1-FO: GCAGCTAATACGACTCACTATAGGTACT GCATGATGTACTTACGTTTTAGAGCTAGAAATAGCAAG	Merck	N/A
T7:sgRNA 2-FO: GCAGCTAATACGACTCACTATAGGGTT GTCGTTACGATTCGTCTGTTTTAGAGCTAGAAATAGCAAG	Merck	N/A
myo1d forward primer [5′ ATCCATGGCGGAACAAAGAGG GGCTGC 3′]	Sigma	N/A
myo1d reverse primer [5′ ATTCTAGATTAATTGGCTGGAAC ACTGAG 3′]	Sigma	N/A
Software and Algorithms		
Adobe Suite CS6: Photoshop and Illustrator	Adobe	N/A
ImageJ/Fiji	N/A	https://fiji.sc/
AxioVision 4.6	Zeiss	N/A
Zen 2012 Blue edition	Zeiss	https://www.zeiss.com
Statistical R-Gui	N/A	https://www.r-project.org/
RStudio	N/A	https://www.rstudio.com/

(*Continued on next page*)

Continued

REAGENT or RESOURCE	SOURCE	IDENTIFIER
Other		
pET100/D-TOPO vector	Invitrogen	N/A
myo1d AUG-MO [5′ TGCAGCCCCTCTTGTTCCGCCATGT 3′]	GeneTools	N/A
myo1d mismatch-MO [5′ TGGACCCCGTCTTCTTCCCC CATGT 3′]	GeneTools	N/A
Axioplan2 imaging microscope	Zeiss	N/A
Zeiss LSM 700	Zeiss	N/A
GloMax® Explorer System	Promega	N/A
AxioCam HSm video camera	Zeiss	N/A
Xenbase	N/A	https://xenbase.org
PubMed	N/A	https://www.ncbi.nlm.nih.gov/pubmed/

CONTACT FOR REAGENT AND RESOURCE SHARING

Further information and requests for resources and reagents should be directed to and will be fulfilled by the Lead Contact, Martin Blum (martin.blum@uni-hohenheim.de).

EXPERIMENTAL MODEL AND SUBJECT DETAIL

For *in vivo* studies, *Xenopus laevis* was used as model organism. Frogs were obtained from Nasco (901 Janesville Avenue PO Box 901 Fort Atkinson). Handling, care and experimental manipulations of animals was approved by the Regional Government Stuttgart, Germany (Vorhaben A379/12 ZO "Molekulare Embryologie"), according to German regulations and laws (§6, article 1, sentence 2, nr. 4 of the animal protection act). Animals were kept at the appropriate condition (pH=7.7, 20°C) at a 12 h light cycle in the animal facility of the Institute of Zoology of the University of Hohenheim. Female frogs (4-20 years old) were stimulated with 25-75 units of human chorionic gonadotropin (hCG; Sigma), depending on weight and age, that was injected subcutaneously one week prior to oviposition. On the day prior to ovulation, female frogs were injected with 300-700 units of hCG. Eggs were collected into a petri dish by careful squeezing of the females, followed by *in vitro* fertilization. Sperm of male frogs was gained by dissecting of testes that were stored at 4°C in 1x MBSH (Modified Barth's Saline with HEPES).

METHOD DETAILS

Plasmid construction

The *myo1d*-CS2+ construct was a gift of Dr. Michael Levin (Tufts University). For generation of a rescue construct, *myo1d* was cloned into the CS2+ myc-tag vector that contained 5 myc sequences at the N terminus. The following primers were used for cloning:

myo1d forward primer: 5′ ATCCATGGCGGAACAAAGAGGGGCTGC 3′
myo1d reverse primer: 5′ ATTCTAGATTAATTGGCTGGAACACTGAG 3′

For *in vitro* synthesis of mRNA using the Ambion sp6 message kit, the plasmid was linearized with NotI.

Immunfluorescence staining

For immunofluorescence staining, embryos were fixed in 4% PFA for 1h at RT on a rocking platform, followed by 2 washes in calcium- and magnesium-free PBS (PBS^-) for 15 min each. For staining of GRP explants, embryos were dissected using a scalpel into anterior and posterior halves. Posterior halves (GRP explants) were collected and transferred to a 24 well plate and washed twice for 15 min in PBST. GRP-explants and whole embryos were blocked for 2h at RT in CAS-Block diluted 1:10 in PBST. The blocking reagent was replaced by antibody solution (anti acetylated tubulin antibody, diluted 1:700 in CAS-Block) and incubated overnight at 4°C. In the morning, the antibody solution was removed and explants/embryos were washed twice for 15 min in PBS^-. Finally, the secondary antibody (diluted 1:1000 in CAS-Block) was added together with Phalloidin (1:200) and incubated for a minimum of 3h at RT. Before photo documentation, embryos or explants were shortly washed in PBS^- and transferred onto a microscope slide.

Flow-analysis

For analysis of leftward flow, dorsal posterior GRP-explants were dissected from stage 16/17 embryos in 1x MBSH [16]. GRP-explants were placed in a Petri dish containing fluorescent microbeads (diameter 0.5 μm; diluted 1:2500 in 1xMBSH) and incubated for a few seconds. Explants were transferred to a microscope slide which was prepared with Vaseline to create a small chamber

that contained fluorescent microbead solution; a coverslip was carefully pressed on to seal the chamber. Time lapse movies of leftward flow were recorded using an AxioCam HSm video camera (Zeiss) at 2 frames per second for 1 min using an Axioplan2 imaging microscope (Zeiss). For flow analysis, two open-source programs, ImageJ and statistical-R, were used. Using the Particle-Tracker plug-in from ImageJ, leftward flow was analyzed and particle movement was measured. Directionality and velocity of fluorescent microbeads were calculated using statistical-R.

Luciferase Assay

Luciferase reporter assays were carried out using the Promega Dual-Luciferase® Reporter Assay System. Embryos were injected at the 4-cell stage with AUG-MO, ATF2-luciferase DNA and Renilla DNA into the dorsal animal blastomeres, and neural tissue was dissected at stage 14/15 (*cf.* Figure S3D for a schematic depiction of the procedure [24];). Neural tissue was transferred into a 1.5 mL Eppendorf tube and the 0.1xMBSH buffer was removed, leaving the tissue moistened. The tissue was lysed and homogenized in 100 μl 1x passive lysis-buffer by pipetting the suspension up and down, followed by a 15 min incubation at RT. The lysate was centrifuged for 2 minutes at 14 000 rpm and the upper phase was transferred into a new tube. The lysate was re-centrifuged and two 25 μl aliquots (technical duplicates) were transferred into a 96well plate. 75 μl 1x Luciferase assay substrate was added through the GloMax® Explorer System and the luminescence was measured. This step was repeated with 75 μl 1x Stop and Glow reagents. To calculate the relative luciferase units (RLU in [%]) the ratio between luciferase and Renilla values was calculated and correlated to the wt control, which we set to 100%.

CRISPR/Cas9 mediated genome editing

sgRNA templates (under T7 promoter control) were generated using Pfu polymerase-mediated primer extension following *in vitro* synthesis (4 h) of the sgRNAs [12]. Prior to use, sgRNAs were denatured at 70°C for 2 min and immediately chilled on ice. Cas9 protein and sgRNAs were mixed and incubated at 37°C for 5 min to allow RNP formation. Zygotes were dejellied 20 min post fertilization and immediately injected with 8 nL of RNP mix. Injected embryos were cultivated for 12 h at 25°C to enhance cutting efficiency, followed by transfer to ambient temperature (20°C) until stage 28 was reached, when specimens were fixed for phenotype analysis.

Monoclonal Antibody Preparation

A monoclonal antibody, Mab4E12, was raised against the tail polypeptide NARNSNQFVSRSNE (aa834-847) of the *Xenopus laevis* myosin 1d L homolog (GenBank Accession Number AF540952.1) by AbPro, Woburn, MA, USA. A 828 bp tail region that included amino acids R729-N1007 was amplified by PCR from a cDNA clone optimized for expression in *E. coli* (GenScrpt), pXIMyo1d-opt, using the primers (Forward: CACCGCCGTTATAAAGTTAAAAGT; Reverse: TTATTAGTTTGCCGGAACAGACAG), and cloned into the pET100/D-TOPO vector (Invitrogen) to create pXIMyo1d-optTail2D. BL21 Star One Shot cells (Invitrogen) were transformed with this vector and expression of the 35 kDa fusion protein consisting of the myo1d tail and N terminus 6X His-tag was induced with IPTG. Cells were harvested after 1.5 hr of induction and the fusion protein was affinity purified using Ni-NTA affinity purification column from a cleared lysate under denaturing conditions (QIAGEN). The affinity purified tail polypeptide was cross-linked to PureProteome NHS Flexibind Magnetic Beads (Milipore), and Mab4E12 was purified following the manufacturer's instructions.

Western blot analysis

Embryos were injected at the 1-4 cell stage with 1 ng of MO and cultivated until stage 28. The antisense morpholino, AUG-MO, [5′ TGCAGCCCCTCTTGTTCCGCCATGT 3′] overlapped the start codon (underlined) of *myo1d*. The control mismatch morpholino MM-MO, [5′ TG**G**A**C**CCC**G**TCTT**C**TTCC**C**CCATGT 3′] was identical to the AUG-MO except for the five C/G mismatches (underlined and indicated by bold lettering). Embryo lysates were made by homogenizing 1 embryo in 20 μl of 4°C lysis buffer (50 mM Tris pH 8.0, 150 mMNaCl, 0.5% NP40 0.5 ml, 0.5% Triton X-100 0.5 ml, 1 mM EGTA) plus cOmplete, Mini, EDTA-free Protease Inhibitor Cocktail (Roche) and centrifuging at 13.000 x g for 10 min to remove cellular debris followed immediately by mixing the supernatant 1:1 with 2x Laemmli SDS sample buffer (SIGMA). Embryo lysates in Laemmli sample buffer were boiled for 5 min, snap cooled on ice, and spun to remove debris before loading onto gels. Bio-Rad Precision Plus Kaleidoscope markers and half-embryo equivalents were loaded per lane on Bio-Rad 4%–20% polyacrylamide precast gels at 100 V. Western blots were prepared using the Trans-Blot SD. Semi-Dry Transfer Cell at 15 V for 45 min. Blots were air-dried, blocked in 5% non-fat dry milk in TBS, rinsed and incubated in the affinity purified 4E12 monoclonal antibody at a concentration of 5 μg in 10 mL TBS overnight at 4°C. Blots were washed in TBS, re-blocked in 10% non-fat dry milk in TBS, rinsed and incubated with goat anti-mouse horseradish peroxidase (HRP) conjugated anti-mouse IgG (Jackson Labs) at 1:10.000 dilution for 1 hr at RT. After rinsing with TBS, chemiluminescent detection was performed using a peroxide-luminol/enhancer solution (Pierce) and GeneSnap image acquisition software on a SynGene gel documentation system.

QUANTIFICATION AND STATISTICAL ANALYSIS

Statistical analysis

Statistical calculations of marker gene expression patterns and cilia distribution were performed using Pearson's chi-square test (Bonferroni corrected) in statistical R. For statistical calculation of ciliation, cilia length, cell size, flow velocity and directionality Wilcoxon-Match-Pair test was used (RStudio).